Electromagnetic Modeling of Aluminium Electrolysis Cells Using Magnetic Vector Potential

Vanderlei Gusberti[1] and Dagoberto S. Severo[2]
1. PhD Engineer
2. Director
CAETE Engenharia Ltda, Porto Alegre, RS, Brazil
Corresponding author: dagoberto@caetebr.com

Abstract

This article presents the numerical simulation of the electromagnetic fields inside the aluminium electrolysis cell and its surroundings using the magnetic vector potential formulation. The finite element commercial code COMSOL was employed both for meshing and solving the numerical model.

Usually, in the previous works, scalar magnetic potential combined with Biot-Savart integration codes was used, often combining 1D and 3D finite elements. Magnetic scalar potential alone is not suitable for the electrolysis cell problem because internal currents are present. It must therefore interact with other codes to add magnetic field generated by free currents in the final magnetic field in an iterative process. Some works also used the integral method to account for the shell shielding combined with Biot-Savart law. The vector magnetic scalar potential however can complete the task in a single step, with the penalty of three times more degrees of freedom. Computational resources and codes have now reached the capacity to allow the use of the complete magnetic vector potential.

The model presented here is able to include the neighbouring lines, steel shell shielding, three dimensional busbars and electrodes, all fully modelled in 3D finite elements, which have to include the surrounding air. The amount of modelled air space necessary to correctly represent the magnetic field bias coming from neighbouring lines is discussed. The modelling results were compared with measurements made in operating cells and with previous magnetic scalar potential results obtained using other software.

Keywords: Aluminium electrolysis cell, magnetohydrodynamics, MHD, magnetic field simulation, magnetic vector potential.

1. Introduction

In aluminium electrolysis cells, the magnetohydrodynamic (MHD) features are determinant factors in the current efficiency and energy efficiency of the electrolysis process. The bath and the liquid aluminum form a system of two immiscible liquids inside the cell cavity. Both liquids are set in motion by the MHD forces (Lorentz forces) produced by magnetic fields coupled with the current densities inside the metal and the bath. If MHD forces in the liquids are too strong and/or asymmetric, the metal pad movement becomes faster, increasing the back-reaction rate and also increasing the risk of metal pad waves. Such undesired disturbances in the process may be controlled by increasing anode-cathode distance (ACD), thus increasing cell voltage and energy consumption. Principles of MHD design of aluminium reduction cells have been laid down in the literature [1] aiming the improvement of magnetic fields features resulting in better cell performance.

The magnetic fields found inside an electrolysis cell can be understood as a superposition of the effects of all conductors surrounding each cell and even the neighbour cell lines. Magnetic field

calculation can be very complex considering the hundreds of conductors, complex busbar geometry and also steel magnetization effect present in potshell, collector bars, anode yokes and superstructure also denominated “magnetic shielding effect”.

2. Evolution of Magnetic Field Calculation in Aluminum Electrolysis Cells

When the cell current and size increased in the 1960’s and 1970’s, it became clear that the MHD of the cell has to be understood and also considered when designing new cell technologies. From that period, one of first magnetic field models can be found [2], where the busbars are approximated as one-dimensional conductors and the shell magnetization effect was considered in the simulation by representing the steel as a collectivity of magnetic dipoles which produce magnetic shielding. This method was used in an in-house code to calculate the magnetic field of the cell for the input to ESTER-PHOENICS commercial code [3].

With development of more affordable computational capacity, models based on Finite Element Method (FEM) became available for electromagnetic field calculation. One approach was to use FEM for the electrical fields inside the studied cell parts combined with Biot-Savart Law integration for magnetic fields (from busbars, neighbouring cells and lines) and the integral equation method to account for steel magnetization. The main advantage of the integral equation method is that the surrounding air and other non-conducting permeable parts do not require to be meshed. This method was used in in-house codes to supply the magnetic field of the cell to ESTER PHOENICS commercial code [4 - 5]. It is also used in MHD-VALDIS [6 - 7].

In 1994, Dupuis and Tabsh [8] developed a procedure to compute magnetic fields in ANSYS. The steel parts and magnetization effects were then included in the FEM model, which required modelling the surrounding air of the cell. ANSYS usually offered four options to calculate magnetic fields:

- Reduced Scalar potential (RSP), solves 1 load step;
- Difference Scalar Potential (DSP) solves 2 load steps;
- Generalized Scalar Potential (GSP) solves 3 load steps;
- Vector potential (VP), solves 1 load step.

Strictly using FEM, the only option to calculate magnetic field in regions where internal currents are present would be the vector potential (VP). Dupuis and Tabsh [8] cited the difficulties in using FEM for the complete magnetic field calculation of the electrolysis cells. At that time, they considered not viable to use the vector potential available in ANSYS due to the following problems:

- All conductors of the studied cell, neighbouring cells and lines required solid 3D mesh. Meshing a large number of parts was considered a time-consuming job.
- Vector potential uses 3 degrees of freedom per node, producing very large finite element matrices, impossible to solve by computers available at that time.
- The amount of modelled air would also increase due to the necessity of enclosing all solid modelled busbars, further increasing the computational requirements.

All scalar potential approaches are suitable only for magnetic domains without electric currents. However, if the magnetic field generated by internal currents is introduced by a source term in each element, GSP [8] could be used for the final cell magnetic field calculation. In ANSYS, it was then possible to use electrical elements (LINK68, SOURCE 36, SOLID5) to calculate currents and afterwards perform a Biot-Savart integration for each element creating the source term of the scalar magnetic potential. The final solution would then be reached in 4 steps: Biot-Savart integration plus the 3 GSP steps. Since the development of the GSP magnetic field

calculation, the ANSYS magnetic scalar potential approach has become a sort of standard way to compute magnetic fields in cells in most of recent works [9 - 12].

Moraru et al [13] calculated magnetic fields inside the electrolysis cell using COMSOL. Their calculation domain was half electrolysis cell geometry. The model included only the most relevant closer busbar of the studied cell with the intention of reducing computational load and meshing work. The results would inevitably be symmetric with respect to the central transverse axis, ignoring important contributions of the neighbouring cells and adjacent lines for the vertical magnetic field (B_z). Despite the important simplifications of the cited model, the work was inspiring as they applied vector potential solution and a future expansion of the calculation domain was suggested.

In this work, we use COMSOL vector potential formulation to calculate a full FEM electromagnetic model of the electrolysis cell, including all important model features necessary to study the cell MHD: internal conductors, steel parts, neighbouring cells, adjacent cell lines, and surrounding air of all conductors.

3. Description of the COMSOL Magnetic Field Model

In order to perform the electrolysis cell magnetic field simulation, the user must have available the COMSOL low frequency electromagnetic package (AC/DC module) in addition to the basic Multiphysics license. When testing the package, we identified some advantages of using COMSOL vector potential approach over the previously used systems at CAETE:

- All parts (busbars, shell, anodic and cathodic assemblies) can be imported from solid modelers such as Solidworks and directly meshed. There is no need for conductors' wireframe modeling or other 1D simplifications of the busbar.
- No Biot-Savart Law integration is required. The solution is performed in single load step. Biot-Savart integration can be very time consuming if the number of nodes increases. This enables finer meshes in conductive parts.
- The COMSOL mesher has proven to be very robust. Complex shell geometry was easily meshed, with minor edition from solid modeler, and more important, all the surrounding air volume was meshed in several minutes. The air can be a complex volume, other softwares have been showing difficulties to perform this task.
- Transition from small scale elements to large scale elements is very important to enable large volume of air required in the VP approach. The mesher performed the required transition of mesh sizes without difficulty.
- The system is easily editable, the user can change the geometry preserving all defined parameters of mesh size, boundary conditions, material definition, model physics, solution setup and post processing features. This greatly reduces the working time when setting up new models if a previous model is available for edition.
- Possibility of coupling electrothermal calculations in the same mesh for busbars and internal cell parts.

The Reynolds P-19 electrolysis cell was chosen to be modelled in this work. The referred cell was running at VALESUL plant (Brazil), dismantled several years ago, see **Figure 25**. CAETE was hired to study MHD improvements for the cell in 2004. At that time, magnetic fields of the cell were measured at a cell current of 168 kA. Magnetic fields were then calculated with ANSYS 9.0 version. In this work, there is the opportunity to compare measured values with the old ANSYS model and with the new COMSOL model.

Figure 25. Reynolds P-19 line at Valesul smelter (shutdown in 2009, currently dismantled).

The **Figure 26** presents the geometry of the studied cell together with adjacent cells and lines ready to be exported for COMSOL use. The adjacent lines and faraway cells can be simplified as single conductors in a similar way of previous models [8 - 9], but with volume instead of wireframe. In **Figure 26**, it is possible to see the distinct geometric scales of the model, from the single cell view up to the whole line view. The air encompassing all the geometry is modelled inside COMSOL environment employing its geometric editor.

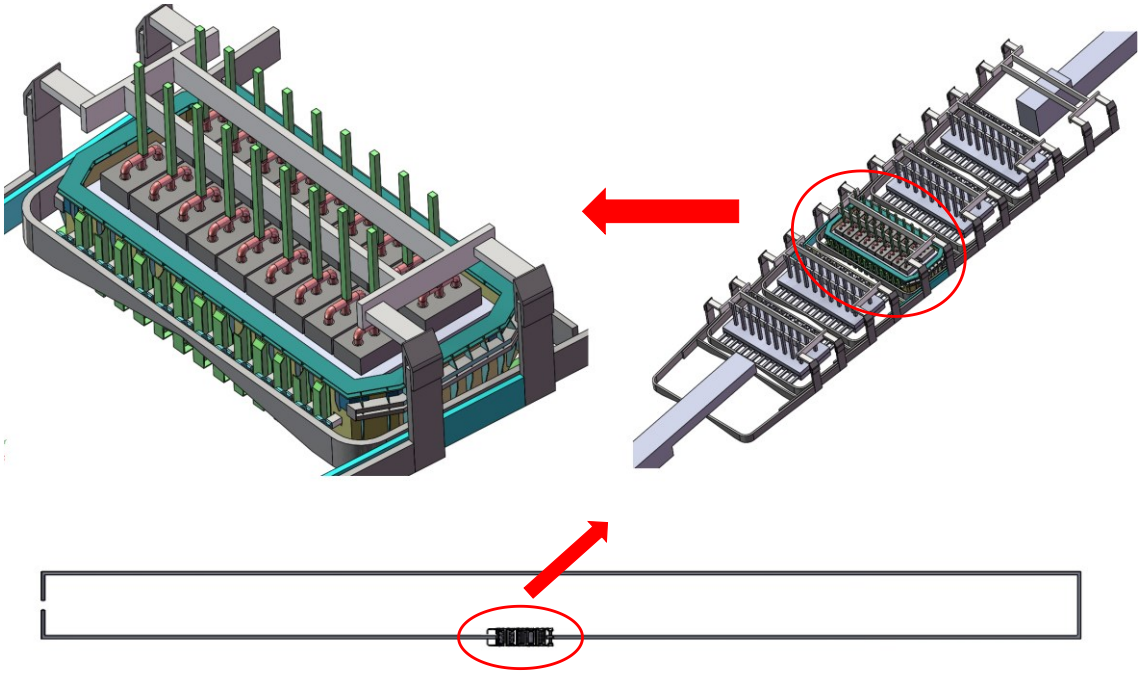

Figure 26: Solidworks geometry ready to export to COMSOL.

Inside COMSOL environment, materials and model physics must be defined. Now the magnetic vector potential is chosen for all domains together with electric potential for conducting solids.

The magnetic vector potential formulation is described by the equations (1) to (7):

$$\nabla \times \mathbf{J} = \mathbf{H} \quad (1)$$
$$\mathbf{B} = \nabla \times \mathbf{A} \quad (2)$$
$$\nabla \times \mathbf{J} = \sigma \mathbf{E} \quad (3)$$
$$\nabla \cdot \mathbf{J} = 0 \quad (4)$$
$$\mathbf{E} = -\nabla V \quad (5)$$
$$\mathbf{B} = \mu_0 \mu_r \mathbf{H} \quad \text{for steel parts} \quad (6)$$
$$\mathbf{B} = \mu_0 \mathbf{H} \quad \text{other domains} \quad (7)$$

where **H** is magnetic field strength, **J** is electric current density, **B** is magnetic flux density, **A** is magnetic vector potential, **E** is the electric field strength, V is electric potential, σ is the electrical conductivity, μ_r is the magnetic permeability of ferromagnetic domains (steel parts), μ_0 is the magnetic permeability of vacuum.

The electric boundary conditions for the model are relatively simple: Total current at the rectifier busbar position of 168 kA (positive pole, Equation (8)) and reference voltage at rectifier position (negative pole, Equation (9)). At the boundaries of electrically conducting domains, electrical insulation is applied, Equation (10). The boundaries of modelled air are treated as magnetic insulation, Equation (11):

Only magnetic fields parallel to the boundary are allowed.

$$\int -\mathbf{n} \cdot \mathbf{J} dA = 168000 \quad (8)$$
$$V = 0 \quad (9)$$
$$\mathbf{n} \cdot \mathbf{J} = 0 \quad (10)$$
$$\nabla \times \mathbf{A} = \mathbf{0} \quad (11)$$

where **n** is the normal vector and $\int dA$ is the surface integration operator.

The steel parts require the definition of the B-H curve. The COMSOL library offers standard B-H curves for steel that can be satisfactorily employed. As a matter of comparison, we decided to use the same curve employed in earlier models.

The modeled air domain must be large enough for the magnetic insulation boundary to be valid. As a consequence, to account for the B_z bias coming from other cell lines, it is required that the air boundary is expanded much beyond the position of the lines. The COMSOL mesh of the expanded air is shown in Figure 27. Around 2 km of air is modelled around the smelter. Various mesh sizes must be handled in the air expansion, starting from spaces near complex solids (shell, anodes, etc.), up to very large elements present in faraway space.

The COMSOL mesher has shown a great level of robustness, the geometry imported from solid modelers (Solidworks) did not require much edition. Transitions from small scale elements to the large scales elements was surprisingly easy. This makes the increase of the domain dimension possible without compromising the number of nodes of the total model. In **Figure 28**, the busbar mesh is shown for the studied cell, two cells at upstream and two cells at downstream. This block of five cells is then connected to a large busbar representing the rest of the line. In **Figure 29**, the

studied cell mesh is shown in more detail. The shell mesh is shown in blue. Ferromagnetic parts require more detailed mesh because of the high nonlinearity of B-H curve.

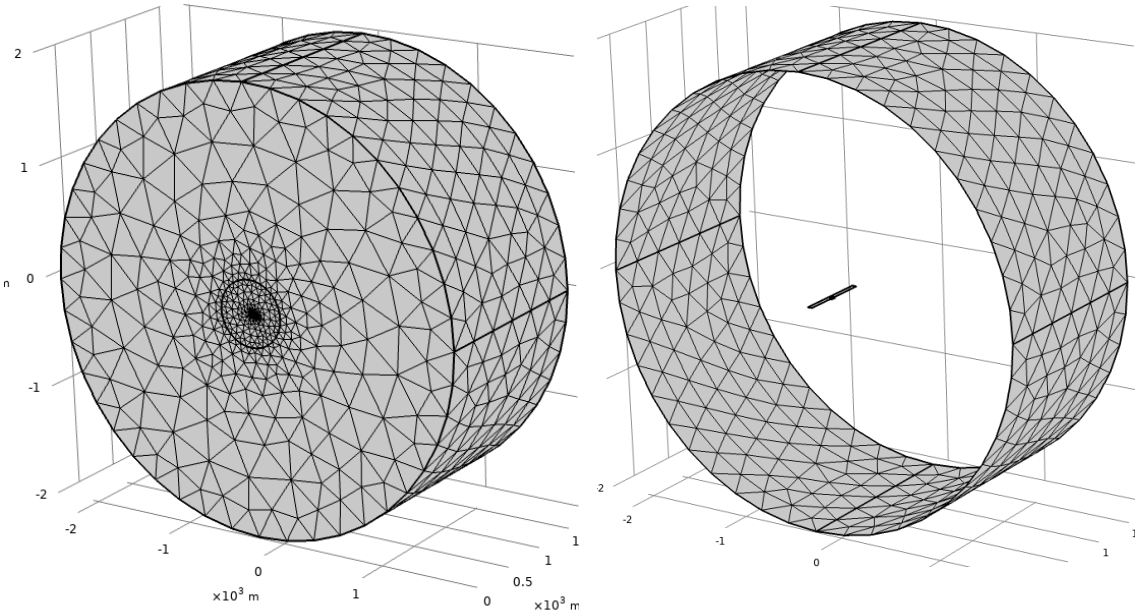

Figure 27. Expanded air mesh. Left: Mesh of expanded air. Right: Cell line size compared with external boundaries of the expanded air.

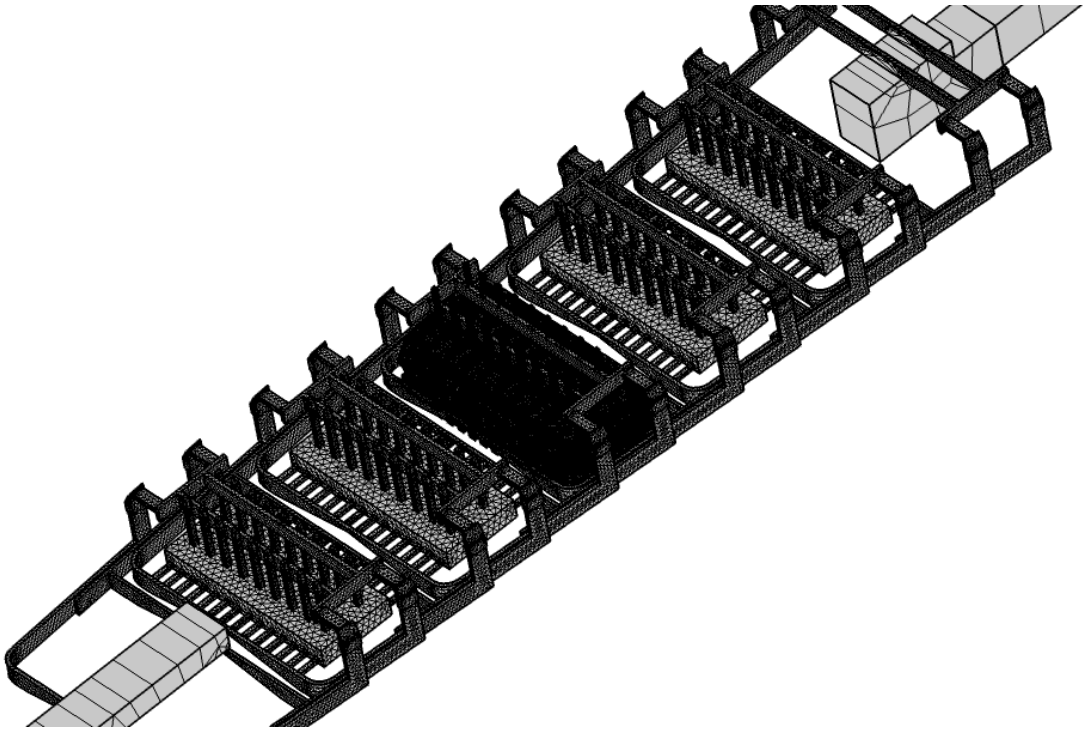

Figure 28. Busbar mesh of neighbouring cells.

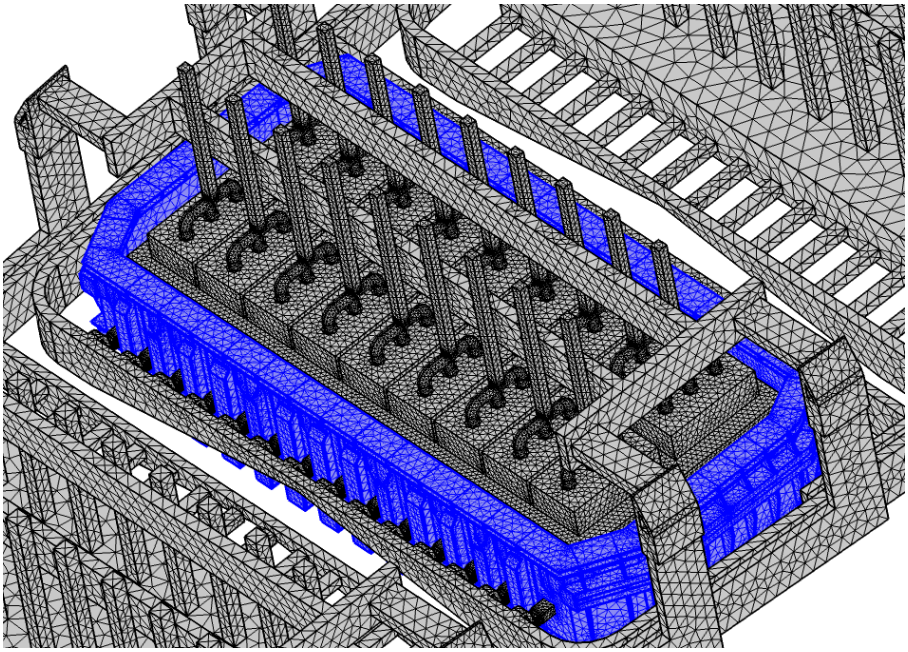

Figure 29. Studied cell mesh, with shell (in blue).

The final mesh resulted in 2.5 million nodes. Using the second order element available in COMSOL, the total number of degrees of freedom reached around 18 million. The model is nonlinear and it must be calculated under iterative solution. The 8-core computer took 2.5 h to solve the model using 35 GB memory (from 64 GB available).

4. Results: Reynolds P19 Cell

In **Figure 30**, magnetization field of the shell parts is shown to illustrate the kind of results achievable with the magnetic modelling. Magnetization is a measure of how a ferromagnetic material responds to the application of a magnetic field (from current carrying parts), also modifying such field (shielding effect). In **Figure 30**, a high degree of magnetization of the shell is seen.

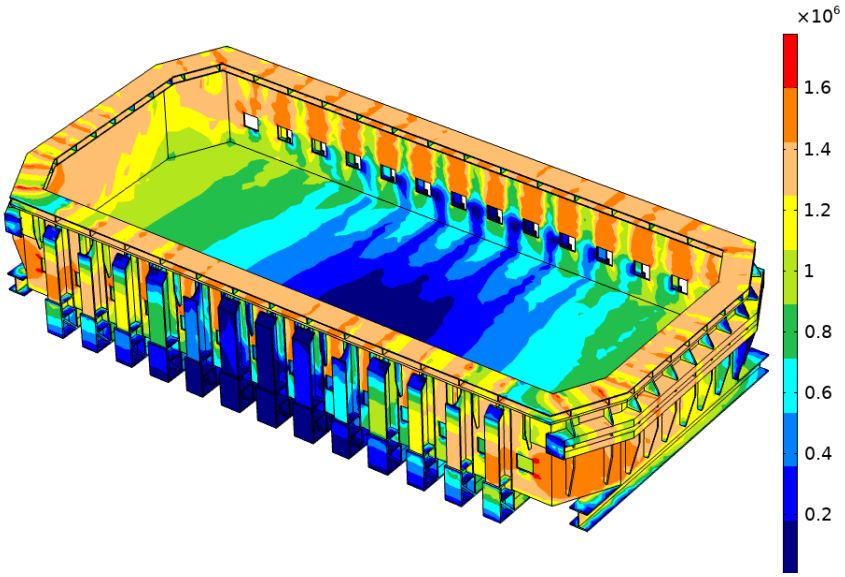

Figure 30. Magnetization field in the shell [A/m].

In
Figure 31, magnetic field calculated in the air around cell lines is shown. This illustrates how the magnetic field propagates from adjacent line towards the studied line.

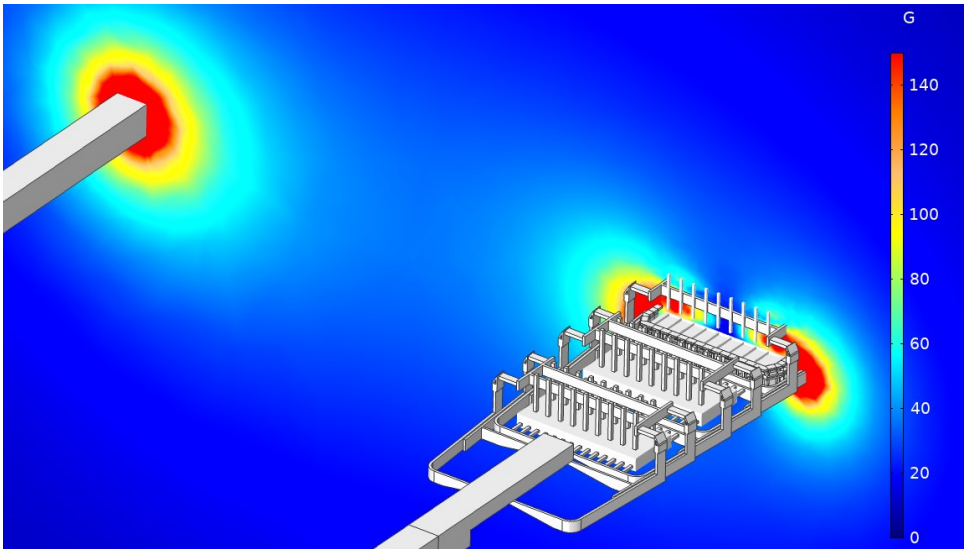

Figure 31. Magnetic flux density magnitude in the air surrounding the cells.

In
Figure 32, a vector plot of magnetic flux density vector **B** inside the metal pad is shown. Stronger magnitudes are found at the corners of the metal pad. The coordinate system convention is: z pointing upwards, y is the current flow direction, from upstream to downstream (from bottom to above in the next pictures) and x is the longitudinal direction (from left to right in the next pictures).

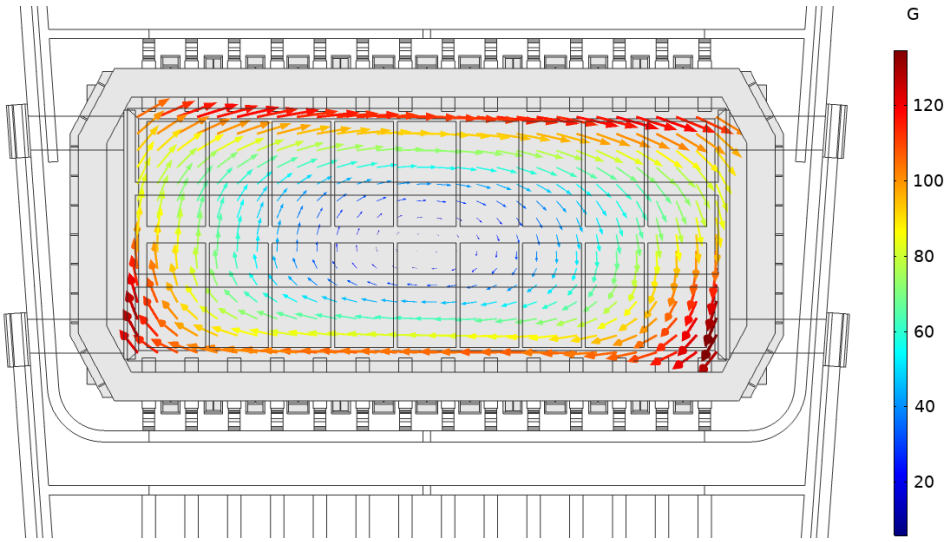

Figure 32. Vector plot of magnetic flux density B inside the metal pad.

The focus of the magnetic analysis is to assess the three components of magnetic flux density **B** inside the metal pad. Especially the vertical component B_z is the most important source of Lorentz forces ($\mathbf{J} \times \mathbf{B}$) that induces metal flow and MHD instability [9]. In the next pictures (**Figure 33**, **Figure 34** and **Figure 35**) the three components of magnetic flux density on the horizontal plane

in the middle of metal pad are shown in contours. The shell wireframe is also shown as geometric reference.

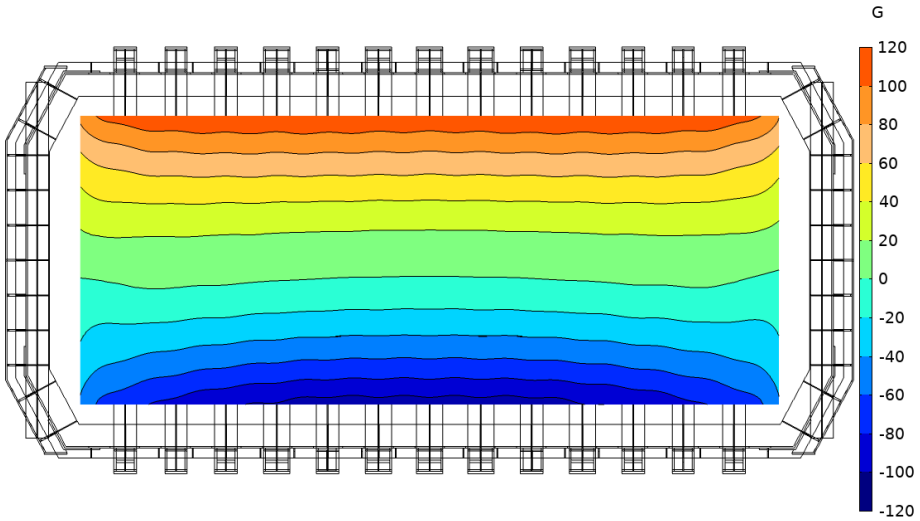

Figure 33. Longitudinal component Bx of magnetic flux density [G].

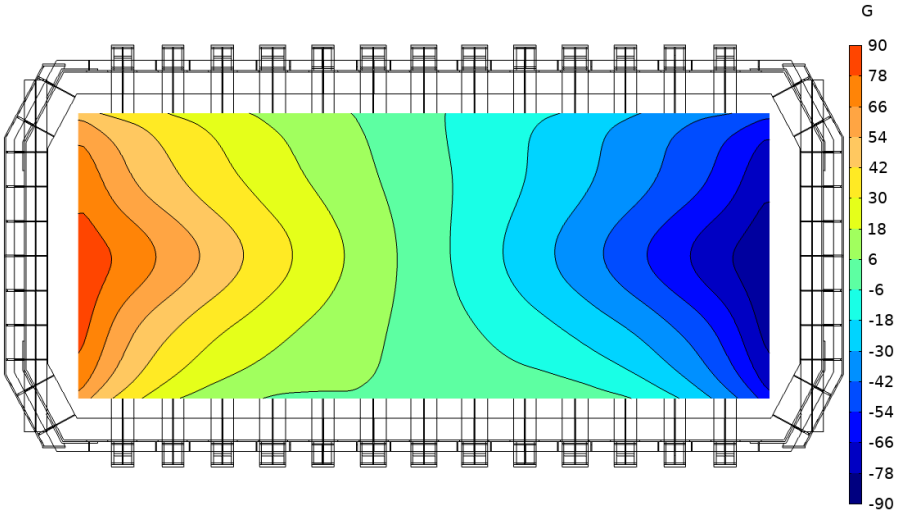

Figure 34. Transversal component By of magnetic flux density [G].

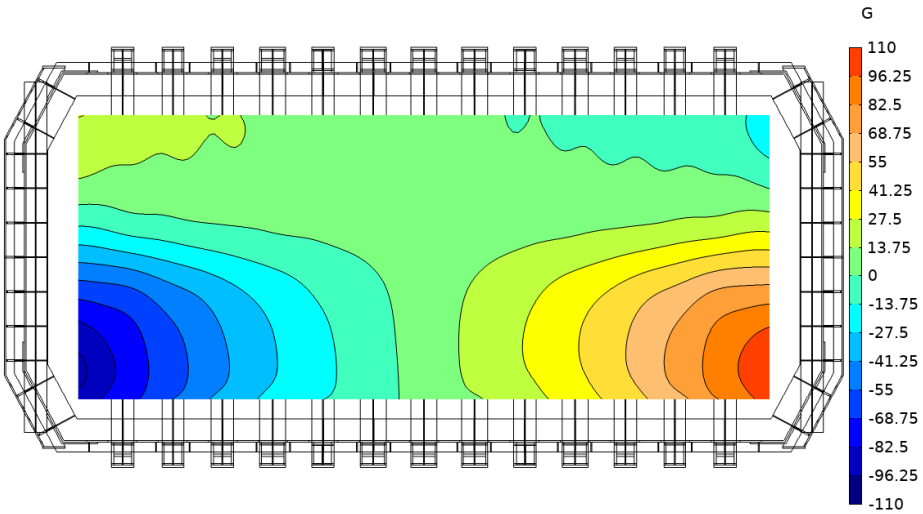

Figure 35: Vertical component Bz of magnetic flux density [G].

The Reynolds P-19 cell is a side-by-side end riser cell. End riser cells are not state of the art for magnetic fields since many decades ago, and the results must be interpreted accordingly.

The most relevant features of the calculated magnetic field are:

- Moderate B_x field, maximum magnitude around 110 G, good symmetry with respect to the x axis. Usually Bx is the highest component in cells;
- High B_y field (comparing with other cell technologies), maximum magnitude around 90 G. Good degree of symmetry. In consequence, metal bath interface deformation is expected to be high.
- Very high B_z when comparing with other cell technologies, maximum magnitude around 110 G. This is expected to occur in end-riser cells. As consequence, the cell is prone to high instability levels and high metal velocity pools as well.

The current densities calculated inside the metal pad are of equal importance to the magnetic fields for an MHD study, because the Lorentz forces are a composition of both fields. The next picture (**Figure 36**) present the three components of current density at the horizontal plane in the middle of the metal pad.

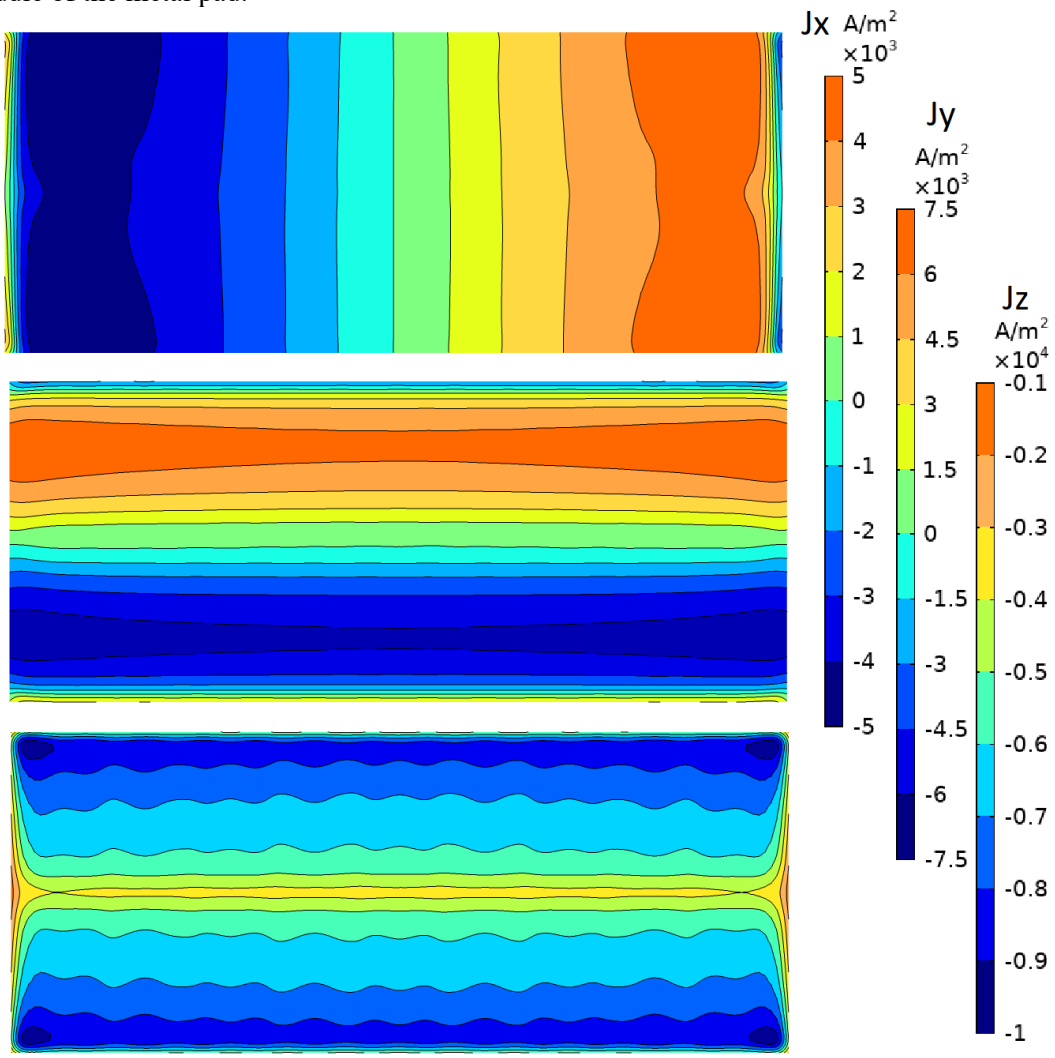

Figure 36. Components of current density at the horizontal plane in the middle of metal pad [A/m^2]. Top: Longitudinal Jx. Middle: Transversal Jy. Bottom Vertical Jz.

The current density patterns present expected features: Current flows downwards, towards the cathode block. Current density pickup at the cathode blocks is higher at the shell sides than in the middle of the cell. This causes horizontal current density to be present in the metal pad as shown in **Figure 36**.

5. Comparison with Measurements in P-19 Cells

The measurements of magnetic flux density were done by CAETE team. The gaussmeter and the tridimensional magnetic probe were developed by CAETE staff in the past and successfully used in many measurement campaigns during the last 15 years. **Figure 37** is a photo of the magnetic flux measurement being performed in a Valesul P-19 electrolysis cell in 2004. In the procedure, the probe is inserted into the cell liquid layers through a hole in the crust. When the probe reaches the metal pad, its coordinate system must be positioned and aligned with the coordinate system attributed to the cell. At this moment, the values for B_x, B_y and B_z are read and recorded. Measurements were taken in many positions at the upstream and downstream of the cell.

Figure 37. Left: Measurements being performed inside the metal pad by CAETE staff employing the magnetic probe. Right: Probe coordinate system.

In the model results, it is possible to pick a line of the results at upstream and at downstream that passes through the positions of the measured points. **Figure 38** shows the comparison between the measured B_x values, COMSOL model results, and ANSYS model results (calculated in 2004) for B_x at the mentioned lines.

In the same manner, **Figure 39** and **Figure 40** show comparisons between measured values and calculated values by COMSOL and ANSYS for B_y and B_z respectively.

The magnetic model is an idealized system. Some deviations from the idealized cell are to be expected due to variations in current density paths inside the cell caused by one or more factors, such as: sludge, anode setting, ledge position non-uniformity, geometry non-uniformities, properties variation, etc.

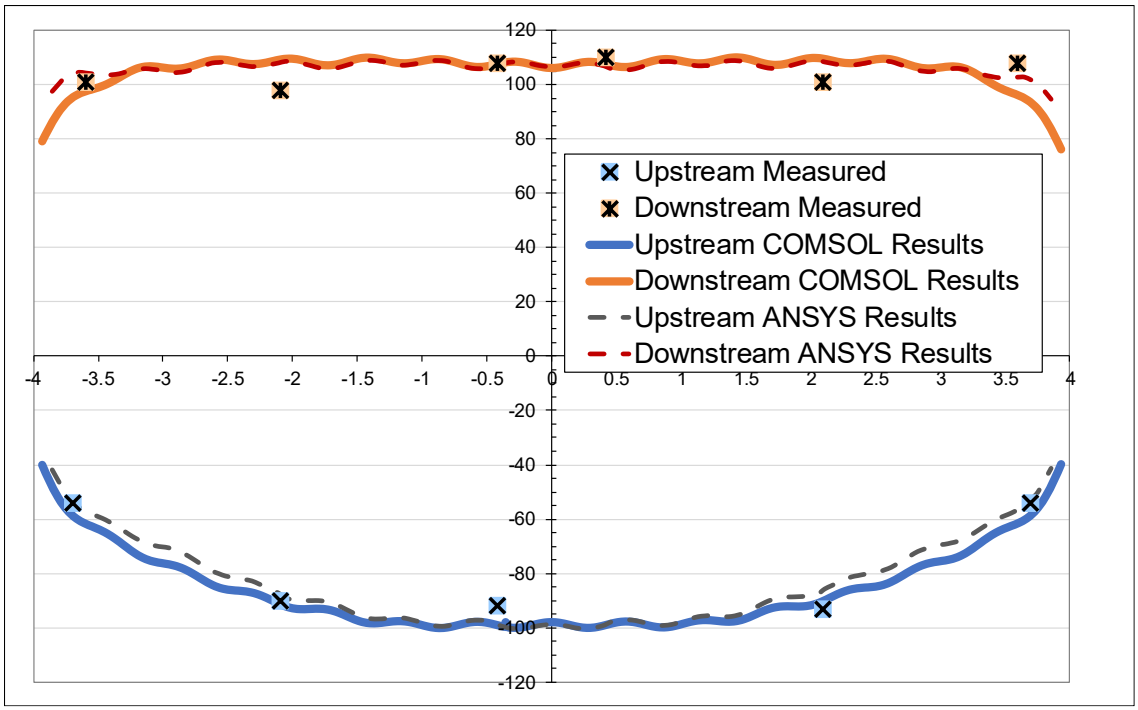

Figure 38. Measured points of Bx compared with calculated values by the COMSOL and ANSYS magnetic models.

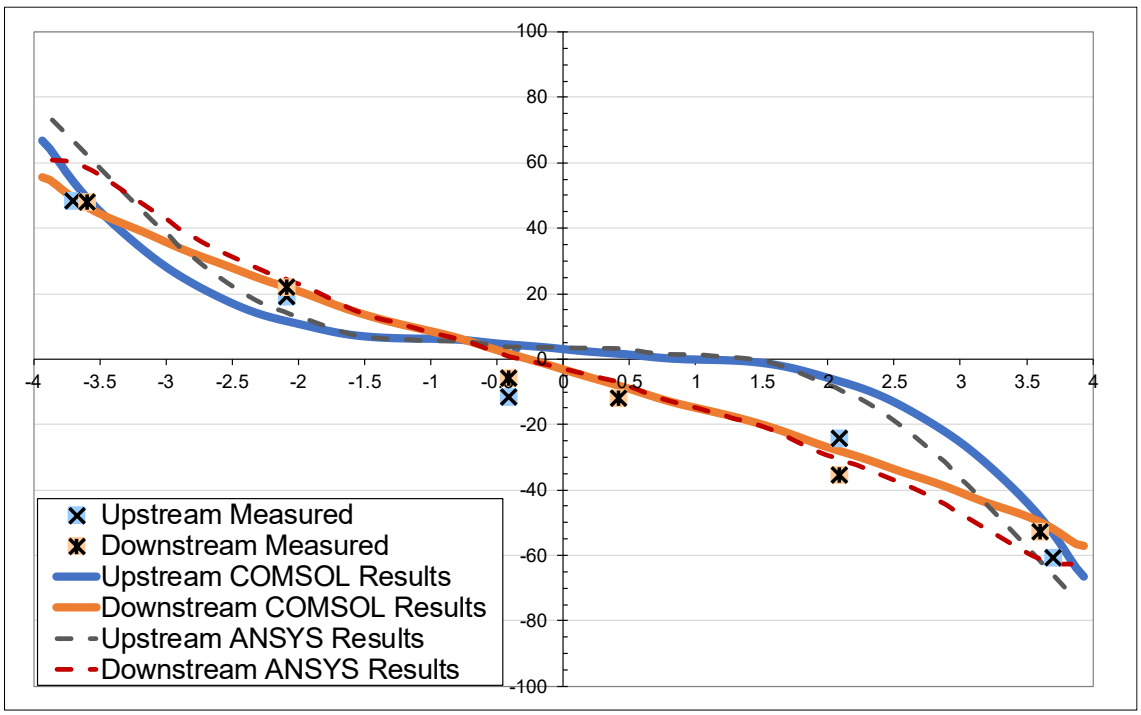

Figure 39: Measured points of By compared with calculated values by the COMSOL and ANSYS magnetic model.

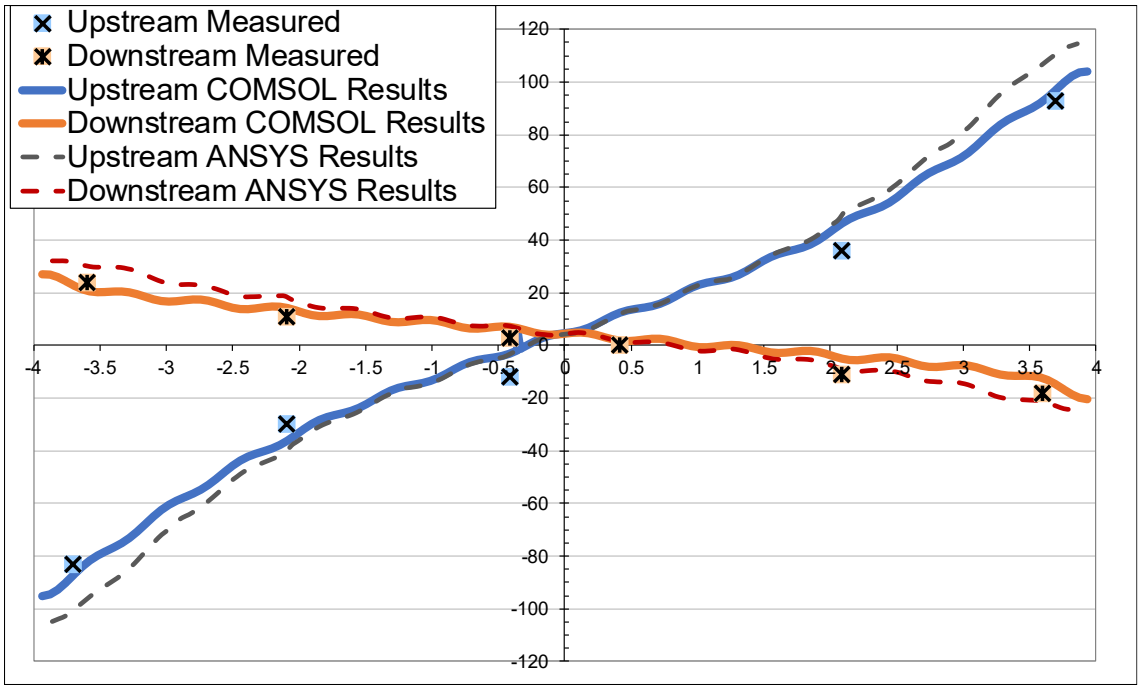

Figure 40. Measured points of B_z compared with calculated values by the COMSOL and ANSYS magnetic model.

Regarding the COMSOL model described in this work, the agreement between model results and measured values is considered to be excellent for B_x and B_z. In The agreement is acceptable for B_y, considering the fact that horizontal current variation caused by anodes primarily affects B_y. The ANSYS model results calculated in 2004 are similar to the COMSOL model results for component B_x, but the ANSYS model seems to overestimate B_y and B_z at the ends of the cell. One reason for the observed difference between the models is that ANSYS model did not consider magnetization of the anode yokes at that time. Only wireframe conductors for these parts were used. As a result, the magnetic attenuation from steel became weaker than in COMSOL model. Another reason for differences could be the use of wireframe conductors in ANSYS instead of volumetric conductors near the shell, changing local magnetization pattern. And, of course, the mesh density used in 2004 was coarser than in the COMSOL model because the personal computers at that time were usually limited to 2 GB memory.

6. Conclusions

Using vector potential approach with FEM to calculate magnetic fields in electrolysis cells was considered a serious challenge in the past. Now, with improvements in software environment and affordable computer capacity, this procedure has become viable as presented in this work.

All important features of the magnetic field assessment have been successfully implemented in the model such as: internal current distribution, steel parts magnetization, neighbouring cell busbars and neighbouring pot rows.

The COMSOL system proved to be very robust. Mesh requirements were satisfied without difficulties. The model is ready for use in other geometries as it can be easily edited and rerun preserving many parametric features.

The studied case is the Reynolds P-19 cell at Valesul. Very good agreement between model results and measurements was found.

7. References

1. Vinko Potočnik, Principles of MHD design of aluminum electrolysis cells. *Light Metals* 1991, 99-105.
2. Thorleif Sele, Computer model for magnetic fields in electrolytic cells including the effect of steel parts, *Light Metals* 1973, 313-319.
3. Vinko Potočnik, Modeling of metal-bath interface waves in Hall-Heroult cells using ESTER/PHOENICS, *Light Metals* 1989, 227-235.
4. Christian Droste, PHOENICS applications in the aluminium smelting industry, *The PHOENICS Journal-Computational Fluid Dynamics and its Applications*, Volume 13 No.1, June 2000, 70-81.
5. Detlef Vogelsang, Application of integrated simulation tools for retrofitting aluminum smelters, *4th Australasian Aluminium Smelting Technology Workshop,* 25th – 30th October 1992, Sydney, Australia, 641-663.
6. Marc Dupuis, Valdis Bojarevics and J. Freibergs, Demonstration thermo-electric and MHD mathematical models of a 500 kA Al electrolysis cell: Part 2, *Light Metals* 2004, 453-459.
7. Abdalla Zarouni, Lalit Mishra, Marwan Bastaki, Amal Al Jasmi, Alexander Arkhipov, Vinko Potocnik, Mathematical model validation of aluminium electrolysis cells at Dubal, *Light Metals* 2013, 597-602.
8. Marc Dupuis, Imad Tabsh, Thermo-electric-magnetic modelling of a Hall-Heróult cell. *Proceedings of the ANSYS Magnetic Symposium* 1994, 9.3-9.13.
9. Dagoberto S. Severo, André-Felipe. Schneider, Elton C. V. Pinto, Vanderlei Gusberti, Vinko Potocnik, Modeling magnetohydrodynamics of aluminum electrolysis cells with ANSYS and CFX*, TMS Light Metals* 2005, 475-480.
10. Amit Gupta, Manoj Chulliparambil, Sankar Namboothiri, Satheesh Mani, Biswat Basu and Jinil Janardhanan, Electromagnetic and MHD study to improve cell performance of an end-to-end 86 kA potline, *Light Metals* 2012, 853-858.
11. Zhiming Liu, Fengquin Liu, Yueyong Wang, Flow field comparison between traditional cell and new structure cell by Chaclo by CFD method, *Light Metals* 2012*,* 955-958.
12. Baokuan Li, Xiaobo Zhang, Sui-rui Zhang, Fang Wang, Nai-xiang Feng, Study of electromagnetic field in 300 kA aluminum reduction cells with innovation cathode structure, *Light Metals* 2011*,* 1029-1033.
13. Augustin Moraru, Alexandru M. Morega, Marin Petre, Marian Cilianu, Magnetohydrodynamic flow in an aluminium electrolysis cell, *Rev. Roum. Sci. Techn. – Électrotechn. et Énerg.* 2011*,* 56*,* 2*,* 131-140.